



Trans. Nonferrous Met. Soc. China 25(2015) 1490-1499

Transactions of Nonferrous Metals Society of China

www.tnmsc.cn



# Effect of solution treatment on corrosion characteristics of biodegradable Mg-6Zn alloy

Seyed Morteza Ghaffari SHAHRI<sup>1</sup>, Mohd Hasbullah IDRIS<sup>1</sup>, Hassan JAFARI<sup>2</sup>, Babak GHOLAMPOUR<sup>1</sup>, Mahtab ASSADIAN<sup>1</sup>

- Department of Materials, Manufacturing and Industrial Engineering, Faculty of Mechanical Engineering, Universiti Teknologi Malaysia, Johor Bahru 81310, Malaysia;
  - 2. Department of Materials Engineering, Faculty of Mechanical Engineering, Shahid Rajaee Teacher Training University, Tehran 16785-136, Iran

Received 30 May 2014; accepted 30 January 2015

**Abstract:** A binary Mg-6Zn biodegradable alloy was solution treated to evaluate the effects of resulting microstructure changes on the alloy's degradation rate and mechanisms in-vitro. The treatment was conducted at 350 °C for 6–48 h. Optical and scanning electron microscopy, energy-dispersive X-ray spectroscopy and X-ray diffraction were used to analyze the as-cast and treated samples. Immersion and electrochemical tests were performed in simulated body fluid at 37 °C to assess the samples corrosion resistance. To confirm the results of the corrosion tests, pH measurement was carried out. It is found that over 24 h solution treatment dissolves intermetallic phases in matrix and produces an almost single phase microstructure. Decreasing the intermetallic phases results in lower cathode/anode region ratios and lowers corrosion rates. The results of the electrochemical and mass loss tests reveal that extended solution treatment improves the corrosion resistance of the alloy. The results also show that solution at 350 °C for 24 h enhances the corrosion resistance of the as-cast alloy more than 60%. In addition, decreasing intermetallic phases in the microstructure accompanied a lower pH rise reduced corrosion rate. Solution treatment is suggested as a corrosion improving process for the application of Mg–Zn alloys as biodegradable implant materials.

Key words: magnesium alloy; solution treatment; biodegradation; immersion; polarization; orthopaedic implant

# 1 Introduction

Degradable biocompatible materials have the potential to play a vital role in load-bearing orthopaedic implants because of the risk of inflammation of non-degradable implants such as stainless steels, titanium-based alloys, and cobalt-chromium alloys [1]. Comparatively, magnesium (Mg) alloys are appealing candidates for biomedical applications because of their unique properties such as light weight, mechanical properties similar to natural bone and noteworthy functions in biological systems [1,2]. Although Mg alloys are susceptible to corrosive environments, especially in the presence of chloride ions (Cl<sup>-</sup>) [3], they have become encouraging biodegradable materials and attracted considerable attention in recent years [4]. The rapid degradation in the electrolytic environment of the human body is the alloys foremost deficiency when used as an orthopaedic implant [5-7]. Magnesium has been alloyed with different elements including aluminium and rare-earth metals to improve its corrosion performance [8]. However, some of the elements added to magnesium are not biocompatible; for instance, aluminium damages osteoblasts and neurons and rare-earth elements lead to hepatotoxicity and inflammation [9-11]. In order to create a biodegradable Mg alloy without toxic side effects, a binary magnesium alloy with 6% (mass fraction) zinc (Mg-6Zn) has been studied and it has been proven to have an acceptable biocompatibility in vitro and in vivo [12,13]. The corrosion resistance of Mg alloys depends not only on alloying elements and content but on the microstructure of the alloy. Different intermetallic structures ( $\beta$ -phase) including MgZn<sub>2</sub>, Mg<sub>2</sub>Zn<sub>3</sub>[14] as well as Mg<sub>7</sub>Zn<sub>3</sub> and Mg<sub>51</sub>Zn<sub>20</sub> have been observed in magnesium-zinc (Mg-Zn) binary alloys during casting solidification. Mg<sub>7</sub>Zn<sub>3</sub> and Mg<sub>51</sub>Zn<sub>20</sub> structures were reported to precipitate at 340 and 325 °C, respectively [15].  $\alpha$ -Mg as the matrix of Mg–Zn alloys has a lower corrosion potential ( $\varphi_{corr}$ ) in comparison with

the  $\beta$ -phase and consequently provides microgalvanic cells. Thus, the matrix corrodes rapidly in corrosive environments [13]. An effective method of heat treatment was reported to alter the microstructure and control the corrosion behaviour of Mg alloys [16]. Studies on Mg-Zn alloys reported that solid solution results in  $\beta$ -phase dissolution into  $\alpha$ -Mg with a more homogeneous microstructure and lower corrosion [17,18]. However, AUNG and ZHOU [19] reported that in AZ91 alloy, solid solution dissolves  $\beta$ -phase into  $\alpha$ -Mg and results in a more homogeneous microstructure that accelerates corrosion phenomenon in the long run. Limited information is available to discuss the effects of solid solution treatment on the biodegradation properties of Mg-Zn alloys. According to Mg-Zn binary phase diagram the maximum zinc (Zn) solid solubility in magnesium is 6.22% at 341 °C [20]. Elevating Zn content increases the corrosion potential of Mg alloy, thus this study aimed to evaluate the effects of solid solution treatment on the biodegradation of Mg-6Zn in-vitro.

# 2 Experimental

#### 2.1 Material preparation

Samples were prepared by casting an alloy with the nominal composition of Mg-6Zn. The alloy was prepared using a commercially pure Mg ingot (99.9%), containing copper and iron impurities less than 0.003%, and high purity Zn granules (99.99%). The melting process was carried out in a mild steel crucible at 700-710 °C in an induction furnace. The melting atmosphere was controlled by pure argon gas. The molten Mg was kept at 700-710 °C for 20 min and then the Zn granules were added while the molten Mg was stirred. The molten Mg-6Zn was maintained at the same temperature for 10 min for the purpose of homogenizing it before it was poured into a cylindrical mild steel mould preheated to 600 °C. The as-cast samples were removed from the mould when they reached room temperature. The as-cast samples were solution treated at 350 °C for 6, 12, 18, 24, and 48 h, respectively and then guenched in water at room temperature. The samples, having dimensions of 10 mm  $\times$  10 mm  $\times$  10 mm were cut from the centre of the as-cast and solution-treated samples and were ground with SiC sand paper up to 1200 grit.

# 2.2 Microstructure characterization

The ground samples were polished with 1  $\mu$ m diamond paste to obtain a mirror surface. Polished samples were etched by an etchant composed of 23 mL methanol, 2 mL nitric acid and 75 mL distilled water for 20 s. Optical microscopy (Nikon Microphot-FXL) and image analysis (Dewinter Biowizard 4.8) were carried

out to characterize the general microstructure of the processed samples. The average grain sizes of the as-cast and solution-treated samples were measured according to the ASTM E112–12 standard. A scanning electron microscope (SEM, Hitachi TM3030) equipped with an energy-dispersive X-ray spectroscope (EDS, Bruker Quantax 70) was used to analyze the elemental distribution of the as-cast samples. Phase composition of the samples was analyzed by X-ray Diffraction (XRD, Siemens–D5000, diffractometer using Cu  $K_{\alpha}$  radiation).

## 2.3 In-vitro degradation evaluation

Electrochemical and immersion tests were performed in a simulated body fluid (SBF) at 37 °C for the in-vitro degradation evaluation of the samples. The SBF used in this work was composed of 8.045 g/L NaCl, 0.355 g/L NaHCO<sub>3</sub>, 0.225 g/L KCl, 0.231 g/L K<sub>2</sub>HPO<sub>4</sub>·3H<sub>2</sub>O, 0.311 g/L MgCl<sub>2</sub>·6H<sub>2</sub>O, 39 mL 1 mol/L HCl, 0.292 g/L CaCl<sub>2</sub> and 0.072 g/L Na<sub>2</sub>SO<sub>4</sub>. TRIS was gradually added until the pH reached 7.4. Table 1 lists the chemical composition of the SBF used in this study and human blood plasma.

**Table 1** Chemical composition of SBF used in this study and human blood plasma [21]

G -1 - (:	Ion concentration/(mmol·L <sup>-1</sup> )								
Solution -	Na <sup>+</sup>	$K^{+}$	Ca <sup>2+</sup>	$Mg^{2^{+}}$	$HCO_3^-$	Cl <sup>-</sup>	$\mathrm{HPO}_4^{2-}$	$SO_4^{2-}$	
SBF	142.2	5.6	2.6	3.2	4.2	191.2	1.3	0.5	
Plasma solution	142.0	5.0	2.5	1.5	27.5	103.0	1.0	0.5	

## 2.3.1 Electrochemical measurement

Electrochemical corrosion test was performed using potentiostat/galvanostat device (Parstat-2263) connected to a laptop with a scan rate of 0.5 mV/s starting from -250 to +250 mV of testing cell instant potential. A standard three-electrode cell consisting of a reference electrode (saturated calomel electrode, SCE), a counter electrode (a graphite rod) and a working electrode (the sample) were set to measure the electrochemical behaviour of the samples. 1 cm<sup>2</sup> of the prepared samples were exposed to 500 mL SBF with a pH of 7.4. The samples were exposed to SBF for 15 min prior to measurement to stabilize their surfaces. SEM was used to evaluate the surface morphologies of the samples after the test.

#### 2.3.2 Immersion test

Mass loss immersion and pH evaluation tests were performed for 240 and 48 h, respectively. The ratio of sample's surface area to SBF volume was kept constant at 0.05 cm<sup>2</sup>/mL according to NACE TM0169/G31–12a in both of the tests. The tests were conducted at 37 °C and pH of the SBF was initially adjusted to be 7.4.

Samples with dimensions of 15 mm  $\times$  12 mm  $\times$  5 mm were ground up to 1200 grit by SiC sand paper and ultrasonically cleaned in acetone for 10 min before the immersion test. The test was conducted in polymer tube with a conical bottom to ensure exposure of all the samples faces to SBF. The SBF used for the mass loss measurement was renewed every 2 h for the first day and every 24 h after the first day to prevent corrosion retardation because of excessive pH elevation. Before renewing the SBF, the pH value was monitored to stay 7.4±0.2 to improve testing accuracy. SEM and XRD analyses were used to examine the corrosion products that formed on the samples. The XRD characterization was performed from  $10^{\circ}$  to  $90^{\circ}$  for  $2\theta$  with  $0.05^{\circ}$  per step. In order to find out the mass loss of the samples, the immersed samples were washed with boiling chromic acid to remove corrosion products. To complement the corrosion analysis, pH evaluation was carried out, although it is not be trusted to reveal an accurate corrosion paradigm [22]. Initially, pH of the SBF was set at 7.4 and then it was recorded at 1, 2, 4, 8, 12, 24, and

48 h after immersion without renewing the SBF.

#### 3 Results and discussion

#### 3.1 Microstructure characterization

Optical micrographs of the as-cast and solution-treated Mg-6Zn alloy samples are illustrated in Fig. 1. Figure 1(a) shows a high density of  $\beta$ -phase distributed mostly along the grain boundaries of the  $\alpha$ -Mg matrix in the as-cast sample. This microstructure is the product of non-equilibrium solidification. Figures 1(b)-(d) show that the  $\beta$ -phase region decreases when the alloy was solution treated for 6, 12, and 18 h, respectively.

The micrographs demonstrated that solution treatment for the aforementioned time spans only dispersed the  $\beta$ -phase precipitates in the microstructure of the Mg-6Zn alloy. Further solution treatments of the alloy for 24 and 48 h resulted in the almost complete dissolution of  $\beta$ -phase and produced a saturated single phase  $\alpha$ -Mg (Figs. 1(e) and (f)). It was observed that the solution treatment led to more homogenous

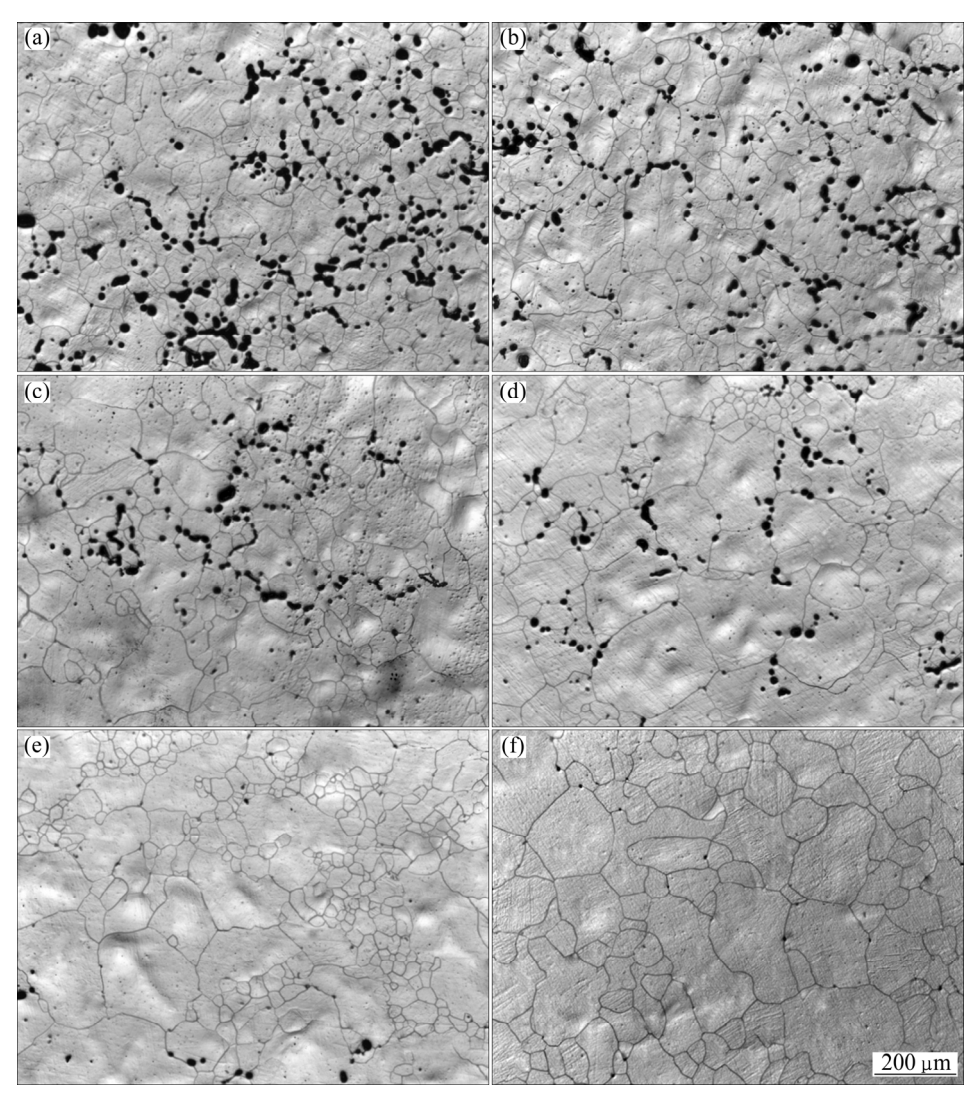


Fig. 1 Optical micrographs of as-cast (a) and solution-treated samples for 6 h (b), 12 h (c), 18 h (d), 24 h (e) and 48 h (f)

microstructure and uniform grain size, which is in agreement with the results reported by GAO and NIE [15]. The homogenous microstructure results from the coalition of  $\beta$ -phase precipitates with the grains. The microstructural changes during solution treatment are  $\beta$ -phases dissolution, fine grain formation, grain shape alteration and final grain growth [23]. The first three changes occur simultaneously. Figures 1(a)–(e) show that when the solution treatment time increases to 24 h only the first three changes occur. This indicates that the solution treatment for 48 h is required to dissolve the  $\beta$ -phase into the  $\alpha$ -Mg and reaches final grain growth.

Figure 2 displays the XRD patterns of the as-cast and solution-treated Mg–6Zn alloy samples. Peaks corresponding to  $\alpha$ -Mg and  $\beta$ -phase were only detected in the samples that were solution treated for less than 24 h. No peaks representing  $\beta$ -phase were observed in the alloy after solution treatment for more than 24 h.

Figure 3 demonstrates the premise that in an as-cast alloy the region located between the  $\beta$ -phase and  $\alpha$ -Mg is Zn-deficient. Figure 3(a) illustrates a schematic demonstration of Zn deficiency and saturation in the as-cast samples. Figure 3(b) represents the SEM image of the as-cast sample and Figs. 3(c) and (d) show the Mg and Zn distribution mapping of the sample, respectively. Due to non-equilibrium solidification and nucleation of  $\alpha$ -Mg which contains less Zn than the molten metal, some high Zn molten metal solidifies as  $\beta$ -phase. The

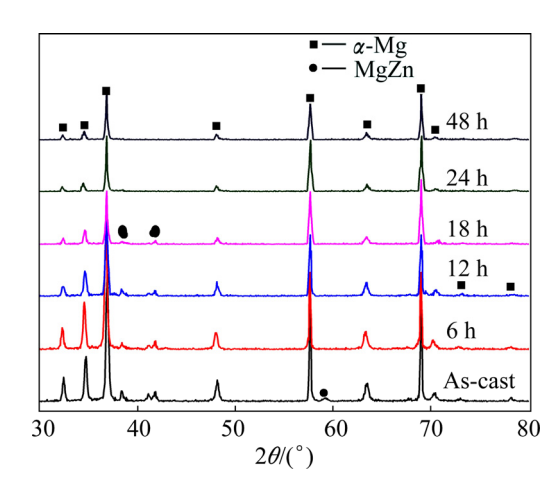


Fig. 2 XRD patterns of as-cast and solution-treated Mg-6Zn allov

authors believe that pre-heating the moulds, which is a casting process requirement, causes a low cooling rate and consequently leads to Zn deficiency. The low cooling rate holds the as-cast samples at temperatures below solvus. The as-cast samples would cool down to temperatures below solvus because of a considerable heat transfer resulted from the high temperature differences. As a result, the Zn content diffuses towards grain boundaries and causes nucleation of further  $\beta$ -phase precipitates. Remarkably, when using slow heating to reach solution treatment temperatures, at the

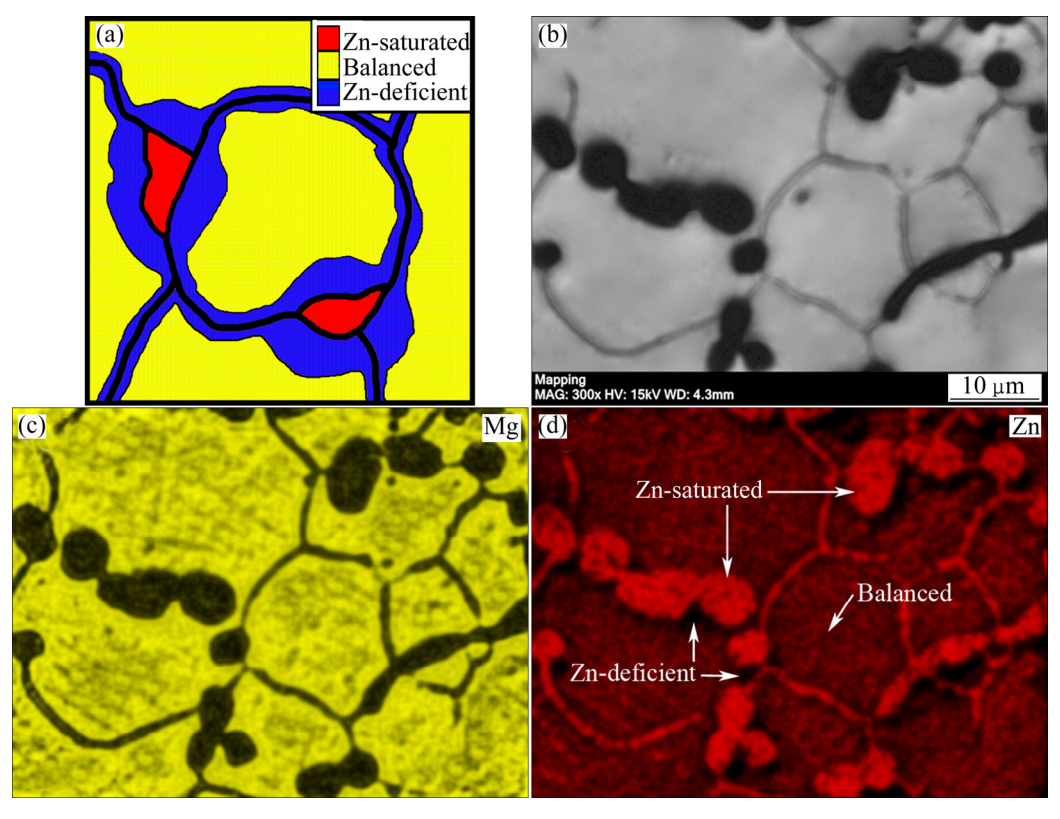


Fig. 3 Zn distribution in microstructure of as-cast samples: (a) Sketch; (b) SEM image; (c) Mg distribution mapping; (d) Zn distribution mapping

temperatures between solidus and solvus, more Zn precipitates towards grain boundaries due to heating below solvus temperature. The  $\alpha$ -Mg at the centre of the grains could be affected by the slow heating but remains consistent because the migration of Zn content from the middle of the grains to the boundary requires a longer heat treating at aging temperatures. Consequently, the region between the centre of the grains and  $\beta$ -phase appreciates, the Zn deficient region, has less Zn comparatively. In short, casting and even solution treatment processes could cause undesirable  $\beta$ -phase precipitates, which could negatively affect the Mg-6Zn properties.

Figure 4 shows the average grain size of the as-cast and solution-treated samples, indicating grain growth after solution treatment. It also illustrates the average intercept number representing the number of grains intersected by random line segments. Figure 4 indicates how the average grain diameter increased by the extension of solution treatment. In addition, it shows how increasing grain diameter accompanies a decrease in the average intercept number. The results indicated approximately 30% increase in grain diameter, from 57 to 73.7 µm, after 24 h. However, extending solution treatment to 48 h indicated less than 10% growth in grain diameter, from 73.7 to 80.6 µm, in comparison to 24 h of the solution treatment. These results are in consistent with microstructure observations implying that 24 h of solution treatment was sufficient to achieve homogenous microstructures. Notably, solution treatment longer than 24 h increased the grain size extensively and may deteriorate the mechanical properties of the alloy.

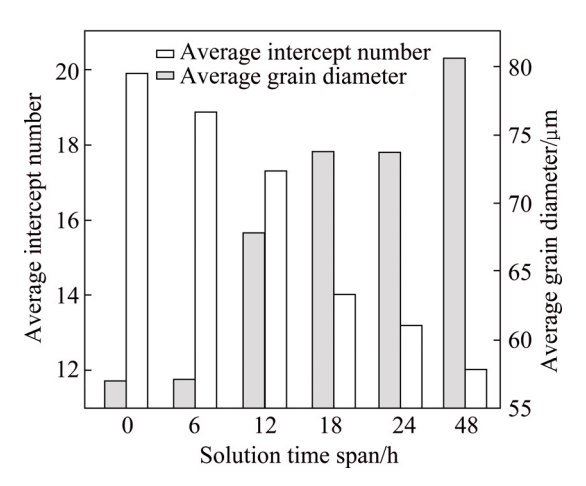


Fig. 4 Average intercept number and grain diameter for as-cast and solution-treated samples

# 3.2 In-vitro degradation results

# 3.2.1 Electrochemical measurement

Figure 5 exhibits the potentiodynamic polarization curves of as-cast and solution-treated samples. The presence of current plateaus in the curves of the as-cast

and solution-treated samples up to 18 h indicates the occurrence of partially protective layers. Similar observations were also reported by ZHANG et al [13]. However, the samples solution treated for 24 h and 48 h do not show any noticeable breakdown potential, which is in agreement with the results reported by SHI et al [24]. The absence of a current plateau implies more protective corrosion layers on the 24 and 48 h solution-treated samples. Eventually, the 24 h and 48 h solution-treated samples have higher cathodic slops that may be the result of the defragmented distribution of Zn in the alloy providing nobler samples over the entire surface. Noticeably, the cathodic polarization curve of all the solution-treated samples demonstrates similar behaviours representing the same electrochemical mechanism for hydrogen evolution through water reduction.

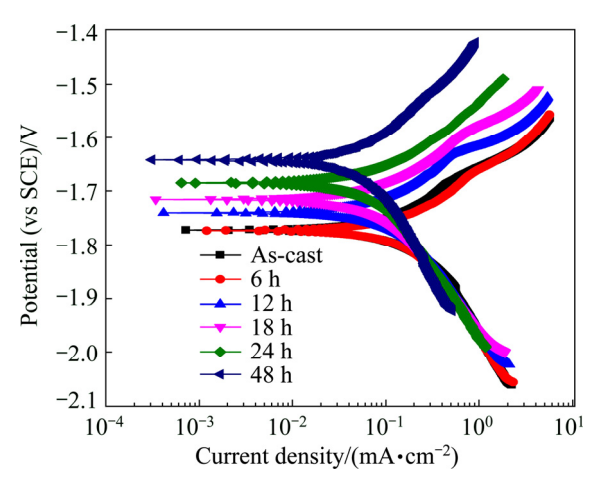


Fig. 5 Polarization curves of samples in SBF at 37 °C

Table 2 summarizes the electrochemical parameters, corrosion current density ( $J_{\rm corr}$ ) and  $\varphi_{\rm corr}$ , as well as the corrosion rate ( $P_{\rm i}$ ) of the samples. Electrochemical curves were used to extrapolate  $J_{\rm corr}$  and  $\varphi_{\rm corr}$ .  $P_{\rm i}$  was calculated according to Eq. (1) [24]. The  $P_{\rm i}$  of the alloy decreases as the time span for the solution treatment increases. Extending the solution treatment time span increases the  $\varphi_{\rm corr}$  of Mg-6Zn alloy. This is highlighted for the 12 and 24 h solution-treated samples that experienced approximately 52% and 72% decrease in  $P_{\rm i}$ 

**Table 2** Corrosion current density, potential and corrosion rate of samples in SBF

or sumpress in SET						
Comple	$\varphi_{\rm corr}({ m vs~SCE})/$	$J_{ m corr}$ /	$P_{\rm i}$ /			
Sample	V	$(mA \cdot cm^{-2})$	$(mm \cdot a^{-1})$			
As-cast	-1.749	0.81	18.51			
6 h solution treated	-1.747	0.63	14.4			
12 h solution treated	-1.723	0.39	8.91			
18 h solution treated	-1.707	0.36	8.23			
24 h solution treated	-1.676	0.23	5.26			
48 h solution treated	-1.651	0.18	4.11			

compared with the as-cast samples, respectively. The decreased  $P_{\rm i}$  indicates that solid solution treatment slightly improved the corrosion resistance of the Mg-6Zn alloy.

$$P_i=22.85J_{corr} \tag{1}$$

Despite grain growth during the solution treatment that is expected to increase the corrosion rate of the alloy, especially the grain growth observed in the 48 h solution-treated sample, lower corrosion rates were observed for the solution-treated samples. This could most probably be ascribed to the dominant effect of coherent Zn distribution in grains, decreasing the cathodic/anodic region ratio. It can be concluded that in some cases, Zn distribution in the Mg–Zn alloys could dominate the corrosion performance of alloy.

Figure 6 displays the surface morphology of the samples after electrochemical measurement. There is a relatively similar pattern between the distribution of dark regions in microstructure (Fig. 1) and the darker areas in micrographs of the electrochemically tested samples. Accordingly, the darker areas on the electrochemically tested samples' morphology probably stem from stabilizing in SBF for 15 min before running the test. The dark areas on the samples' morphology represent an alloy

with low Zn content that was rapidly corroded during stabilizing. In addition, there are a few aggressively corroded spots shown in Figs. 6(a)–(d) probably indicating the presence of less Zn in the area (based on the premise demonstrated in Fig. 3). Interestingly, extremely corroded areas of the tested samples are restricted to the darker areas. In Fig. 6(a), the corrosion products cover the darker area suggesting an inefficient protective layer and passivation on the as-cast sample. Notably, in Fig. 6(b) the corrosion on the darker area is limited. There are restricted dark areas in Figs. 6(c) and (d), and corrosion products are restricted to some areas. 3.2.2 pH evaluation results

In order to complement the results obtained from the electrochemical measurement, immersion test was performed. The result of pH measurement during the test is illustrated in Fig. 7. It is shown that the pH values increased sharply from 7.4 to 8.2–8.3 in the first 8 h. The initial pH rise is attributed to rapid hydrogen (H<sub>2</sub>) evolution and hydroxyl (OH<sup>-</sup>) accumulation in SBF. OH<sup>-</sup> is the product of Mg corrosion in the environments containing Cl<sup>-</sup>. Reactions (2)–(6) describe the series of anodic and cathodic reactions which lead to OH<sup>-</sup> accumulation and hydrogen evolution. Reactions (2) and (3) show the basic anodic and cathodic reactions at the

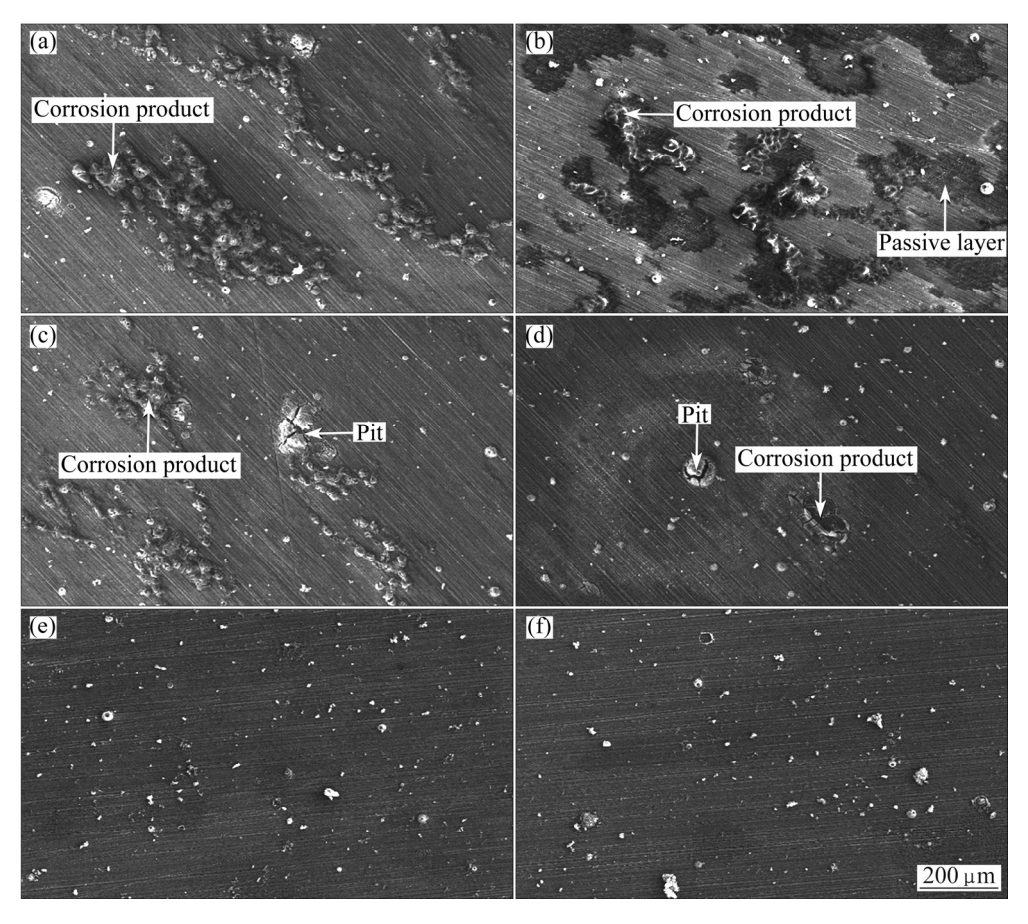


**Fig. 6** SEM images showing surface morphologies of potentiodynamic tested samples in SBF solution treated for different time: (a) As-cast; (b) 6 h; (c) 12 h; (d) 18 h; (e) 24 h; (f) 48 h

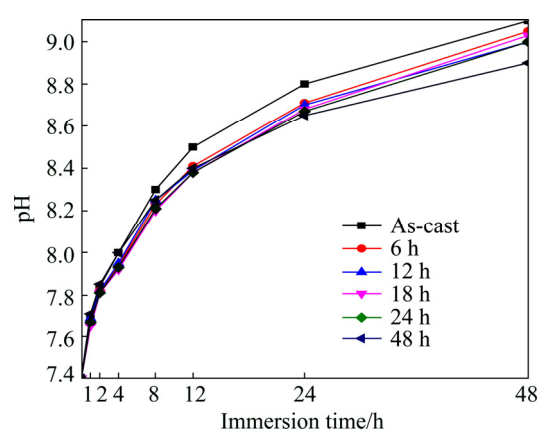


Fig. 7 pH values of SBF after 48 h immersion of as-cast and solution-treated samples

sample–SBF interface which convert Mg and water to magnesium ions (Mg<sup>2+</sup>), OH<sup>-</sup> and H<sub>2</sub>. Reaction (4) shows how the resulted ions react chemically to form a corrosion product, magnesium hydroxide (Mg(OH)<sub>2</sub>). H<sub>2</sub> evolution results from the accretion of OH<sup>-</sup> in the form of Mg(OH)<sub>2</sub> on the surface of sample. Reaction (5) describes the replacement of OH<sup>-</sup> with Cl<sup>-</sup>, which releases OH<sup>-</sup> into SBF and consequently increases pH. However, magnesium chloride, MgCl<sub>2</sub>, is an unstable compound and dissolves easily in SBF, releasing Cl<sup>-</sup> into SBF (Reaction (6)). Thus, there is always Cl<sup>-</sup> in SBF to attack Mg(OH)<sub>2</sub> and release more OH<sup>-</sup> that, in turn continuously increases the pH of SBF.

$$Mg \rightarrow Mg^{2+} + 2e$$
 (Anodic reaction) (2)

$$2H_2O+2e \rightarrow H_2+2OH^-$$
 (Cathodic reaction) (3)

$$Mg^{2+} + 2OH^{-} \rightarrow Mg(OH)_{2}$$
 (4)

$$Mg(OH)_2 + Cl^- \rightarrow MgCl_2 + OH^-$$
 (5)

$$MgCl_2 \rightarrow Mg^{2+} + Cl^-$$
 (6)

The pH of SBF should rise significantly and uncontrollably due to Mg corrosion; however, there are some obstacles that retard pH rise. Firstly, increasing pH and OH concentration leads to Mg(OH)2 stabilization. The stabilized Mg(OH)<sub>2</sub> protects Mg against corrosion by hindering Mg diffusion into SBF and retarding pH Secondly, tertiary magnesium phosphate  $(Mg_3(PO_4)_2)$  could occur in the presence of  $HPO_4^{2-}$  at the early stages of Mg corrosion and low OHconcentration [25]. However, it is reported that the pH rise introduces new opportunities for further Mg<sub>3</sub>(PO<sub>4</sub>)<sub>2</sub> accumulation the surface on samples' Simultaneously, the presence of calcium ions (Ca<sup>2+</sup>) and phosphate (PO<sub>4</sub><sup>3-</sup>), Mg<sup>2+</sup> and OH<sup>-</sup> in SBF contributes to the nucleation and the growth of various calciumphosphate composite (Ca-P composition) structures on  $Mg(OH)_2$  [25–27]. However, there is  $HCO_3^-$  in the SBF. It is improbable that even minute amounts of magnesium

carbonate (MgCO<sub>3</sub>) precipitate onto the samples. MgCO<sub>3</sub> forms either in pH above 9.3 [25] or at high concentrations of HCO<sub>3</sub> in SBF [26]. Thus, the pH rise retardation in this study could not be resulted from the precipitation of highly insoluble MgCO<sub>3</sub> onto the surface of samples.

Based on Fig. 7, although similar pH variation behaviour can be seen for all samples, pH rise rates for solution-treated samples are retarded, especially in the 48 h solution-treated sample. The pH values of the SBF in which the as-cast, 6 h and 48 h solution-treated samples were immersed were recorded at 9.1, 9.05 and 8.9, respectively. Therefore, solid solution treatment may decrease the degradation rate of Mg–6Zn magnesium implants and control pH variation.

#### 3.2.3 Mass loss results

Table 3 shows the mass loss and corrosion rate ( $P_{\rm w}$ ) results of the samples after immersion in SBF for 240 h.  $P_{\rm w}$  is calculated according to Eq. (7) [24]. Table 3 depicts the as-cast and the 48 h solution-treated samples as the most and the least corroded samples, respectively. The  $P_{\rm w}$  values of the 48 h solution-treated and the as-cast samples were calculated as 14.07 and 35.91 mm/a, respectively. The high  $P_{\rm w}$  of the as-cast sample suggests aggressive corrosion, which is the result of high potential difference between the  $\beta$ -phase and the adjacent Zn-deficient microstructure as well as the high ratio of the cathode/anode region.

**Table 3** Mass loss ( $\Delta m$ ) and corrosion rate of samples after immersion in SBF for 240 h

Sample	$\Delta m/$ (mg·cm <sup>-2</sup> ·d <sup>-1</sup> )	Corrosion rate, $P_{\rm w}/({\rm mm \cdot a^{-1}})$	
As-cast	17.1	35.91	
6 h solution treated	11.0	23.10	
12 h solution treated	10.2	21.42	
18 h solution treated	8.7	18.27	
24 h solution treated	7.1	14.91	
48 h solution treated	6.7	14.07	

In other words, the  $\beta$ -phase in the as-cast sample not only resulted in a larger cathodic region, but also an intensively reactive microstructure. Mass loss results represent around 61% decrease in  $P_{\rm w}$ . It should be noted that the 24 h solution treated sample shows almost similar corrosion rate to the 48 h solution treated sample. Therefore, it can be claimed that although the solution treatment contributes to lower corrosion rates in Mg-6Zn alloy, sufficient solution time spans are required to achieve the best result.

$$P_{\rm w}=2.10\Delta m \tag{7}$$

Because Mg corrosion is composed of both

electrochemical and chemical reactions, electrochemical tests are expected to assess  $P_i$  lower than  $P_w$  [28]. Although,  $P_i$  correlates with  $P_w$ , they do not follow the same proportions. Figure 8 comparatively illustrates  $P_i$ and  $P_{\rm w}$  and the difference between  $P_{\rm i}$  and  $P_{\rm w}$  ( $P_{\rm i}$ – $P_{\rm w}$ ). It is clear that solution treatment decreases  $P_i$ – $P_w$ . It should be noticed that apart from the as-cast and 6 h solution-treated samples,  $P_i$ - $P_w$  is larger than  $P_i$ . It could be concluded that the corrosion rate of solution-treated samples for more than 6 h could not be precisely assessed by the electrochemical method. As well, it can be stated that solution treatment decreases the electrochemical reactions involved in Mg-6Zn alloy corrosion. The decrease in the electrochemical portions of corrosion might be directly related to the changes in the samples' microstructure that reduces microgalvanic cells. Generally, Fig. 8 indicates that although the electrochemical method, Tafel extrapolation, gives correct relative results, it does not provide reliable corrosion rate. Finally, it should be remarked that long-term corrosion tests reveal the real corrosion performance of Mg alloys.

Figure 9 demonstrates the surface morphologies of as-cast and solution-treated samples after immersion in SBF for 240 h. Figure 9(a) shows white corrosion

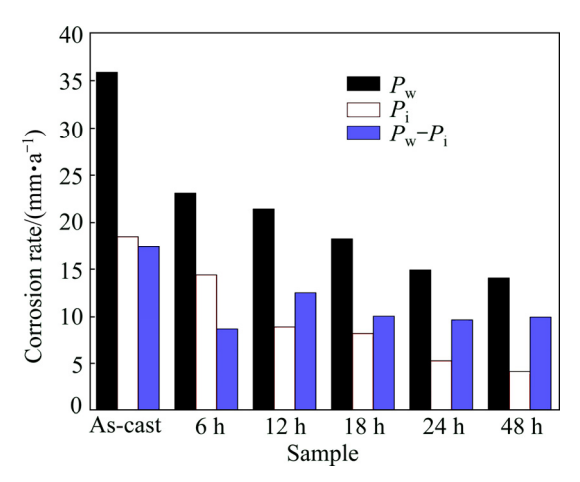


**Fig. 8**  $P_{\rm w}$ ,  $P_{\rm i}$  and  $P_{\rm w}$ – $P_{\rm i}$  of as-cast and solution-treated samples

products with deep and broad cracks formed on the surface of the as-cast sample, while Fig. 9(b) represents formation of smaller amounts of corrosion products on the 6 h treated sample. The white corrosion products may be Ca–P compositions although with the accuracy of this study it could not be stated for certain. The presence of broad cracks in all of the samples' corrosion products can be attributed to dried corrosion products such as Mg(OH)<sub>2</sub> and Ca–P compositions. Figures 9(c) and (d)

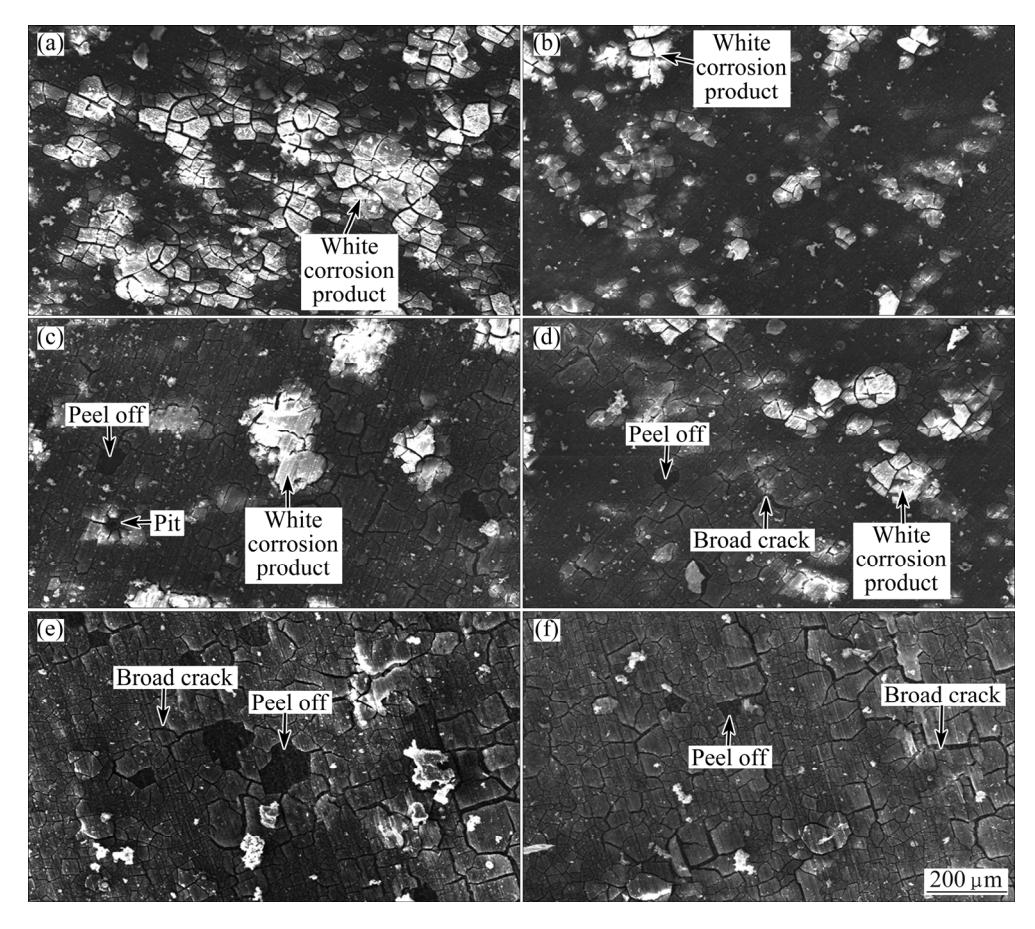


Fig. 9 Morphologies of surface after 240 h immersion in SBF for as-cast (a), 6 h (b), 12 h (c), 18 h (d), 24 h (e), and 48 h (f) solution-treated samples

represent the surface of samples solution-treated for 12 h and 18 h, respectively after the immersion test. The 12 h and 18 h solution-treated samples showed almost similar corrosion features such as broad cracks, peeled off corrosion products and pits. On the other hand, the 24 h and 48 h solution-treated samples shown in Figs. 9(e) and (f) respectively showed less corrosion susceptibility as indicated by the formation of less white corrosion products. The smaller corrosion product formation can be attributed to a less aggressive and localized corrosion resulting from the homogenous microstructure.

Figure 10 displays the XRD patterns of samples after the mass loss immersion test. The patterns indicate the presence of Mg as well as Mg(OH)2 and Ca-P compositions. The as-cast sample showed broad Mg(OH)<sub>2</sub> peaks in comparison with the other samples. In contrast, the Mg(OH)<sub>2</sub> peaks in XRD patterns of the solution-treated samples were more intense than those of the as-cast sample. Mostly, the peaks corresponding to Mg became more intense with extending solution treatment time. The intense Mg peaks in the patterns corresponding to solution-treated samples probably stem from the broad cracks in the corrosion products and peel offs. Although with the accuracy of the current study no distinct peaks corresponding to Ca-P composition were detected, careful analysis of the patterns revealed minor peaks at  $2\theta$  of  $28.68^{\circ}$ ,  $32.05^{\circ}$ ,  $42.40^{\circ}$  and  $46.78^{\circ}$ , indicating the presence of Ca-P compositions. Accumulation of Ca-P compositions could be retarded or even hindered by the uniform accumulation of Mg(OH)<sub>2</sub> at the initial stage of the degradation process. Uniform Mg(OH)<sub>2</sub> accumulation, although susceptible to Cl attacks could avoid the localized and aggressive pH rise required for Ca-P composition precipitation.

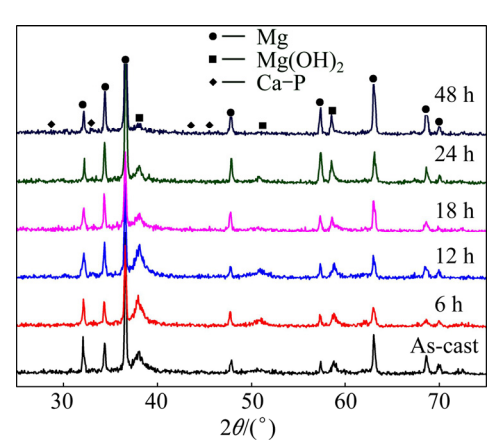


Fig. 10 XRD patterns of samples after immersion in SBF for 240 h

# **4 Conclusions**

1) Solution treatment at 350 °C can lead to a

complete solution of  $\beta$ -phase and result in an almost single phase microstructure as well as uniform grain size after 24 h.

- 2) Solid solution treatment results in a slight decrease in corrosion rates as a result of the uniform distribution of cathodic ( $\beta$ -phase) and anodic ( $\alpha$ -Mg) phases as well as a lower cathode/anode region ratio or even the elimination of cathode phase in the samples.
- 3) The pH value of SBF is decreased by solution treatment of Mg-6Zn alloy, indicating lower corrosion rate for the solution-treated alloy.
- 4) Solution treatment for 24 h reveals approximately 61% and 72% decrease in mass loss and corrosion current density in SBF, respectively, suggesting the treatment is an effective process for the manufacturing of the Mg-6Zn implant alloy.

# Acknowledgements

The authors are grateful for the Ministry of Higher Education of Malaysia for the financial support (Vote No. Q.J130000.2524.04H18) and Faculty of Mechanical Engineering of Universiti Teknologi Malaysia (UTM) for providing research facilities.

#### References

- STAIGER M P, PIETAK A M, HUADMAI J, DIAS G. Magnesium and its alloys as orthopedic biomaterials: A review [J]. Biomaterials, 2006, 27: 1728–1734.
- [2] SHI Guo-liang, ZHANG Ding-fei, ZHANG Hong-ju, ZHAO Xia-bing, QI Fu-gang, ZHANG Kui. Influence of pre-deformation on age-hardening response and mechanical properties of extruded Mg-6%Zn-1%Mn alloy [J]. Transactions of Nonferrous Metals Society of China, 2013, 23: 586-592.
- [3] ZENG Rong-chang, ZHANG Jin, HUANG Wei-jiu, DIETZEL W, KAINER K, BLAWERT C, WEI Ke. Review of studies on corrosion of magnesium alloys [J]. Transactions of Nonferrous Metals Society of China, 2006, 16(S): s763-s771.
- [4] GU Yan-hong, CAI Xiao-jun, GUO Yuan-jun, NING Cheng-yun. Effect of chloride ion level on the corrosion performance of MAO modified AZ31 alloy in NaCl solutions [J]. Materials & Design, 2013, 43: 542–548.
- [5] SONG Guang-ling, ATRENS A, WU Xian-liang, ZHANG Bo. Corrosion behaviour of AZ21, AZ501 and AZ91 in sodium chloride [J]. Corrosion Science, 1998, 40: 1769–1791.
- [6] ZHOU Wei, SHEN Tian, AUNG N N. Effect of heat treatment on corrosion behaviour of magnesium alloy AZ91D in simulated body fluid [J]. Corrosion Science, 2010, 52: 1035–1041.
- [7] WITTE F, KAESE V, HAFERKAMP H, SWITZER E, MEYER-LINDENBERG A, WIRTH C J, WINDHAGEN H. In vivo corrosion of four magnesium alloys and the associated bone response [J]. Biomaterials, 2005, 26: 3557–3563.
- [8] ZENG Rong-chang, DIETZEL W, WITTE F, HORT N, BLAWERT C. Progress and challenge for magnesium alloys as biomaterials [J]. Advanced Engineering Materials B, 2008, 10: 3-14.
- [9] ZHANG Shao-xiang, LI Jia-nan, SONG Yang, ZHAO Chang-li, ZHANG Xiao-nong, XIE Chao-ying, ZHANG Yan, TAO Hai-rong, HE Yao-hua, JIANG Yao. In vitro degradation, hemolysis and MC3T3-E1 cell adhesion of biodegradable Mg–Zn alloy [J].

- Materials Science and Engineering C, 2009, 29: 1907-1912.
- [10] SUN Yu, KONG Min-xiu, JIAO Xiao-hui. In-vitro evaluation of Mg-4.0Zn-0.2 Ca alloy for biomedical application [J]. Transactions of Nonferrous Metals Society of China, 2011, 21(S2): s252-s257.
- [11] DRYNDA A, DEINET N, BRAUN N, PEUSTER M. Rare earth metals used in biodegradable magnesium—Based stents do not interfere with proliferation of smooth muscle cells but do induce the upregulation of inflammatory genes [J]. Journal of Biomedical Materials Research (Part A), 2009, 91: 360–369.
- [12] SONG Guang-ling. Control of biodegradation of biocompatable magnesium alloys [J]. Corrosion Science, 2007, 49: 1696–1701.
- [13] ZHANG Shao-xiang, ZHANG Xiao-nong, ZHAO Chang-li, LI Jia-nan, SONG Yang, XIE Chao-ying, TAO Hai-rong, ZHANG Yan, HE Yao-hua, JIANG Yao. Research on an Mg–Zn alloy as a degradable biomaterial [J]. Acta Biomaterialia, 2010, 6: 626–640.
- [14] ZENG Rong-chang, KAINER K U, BLAWERT C, DIETZEL W. Corrosion of an extruded magnesium alloy ZK60 component—The role of microstructural features [J]. Journal of Alloys and Compounds, 2011. 509: 4462–4469.
- [15] GAO Xiang, NIE J F. Structure and thermal stability of primary intermetallic particles in an Mg–Zn casting alloy [J]. Scripta Materialia, 2007, 57: 655–658.
- [16] ZENG Rong-chang, HAN En-hou, KE Wei. Corrosion of artificial aged magnesium alloy AZ80 in 3.5 wt pct NaCl solutions [J]. Journal of Materials Science and Technology, 2007, 23: 353–358.
- [17] ZHANG Shao-xiang, LI Jia-nan, SONG Yang, ZHAO Chang-li, XIE Chao-ying, ZHANG Xiao-nong. Influence of heat treatments on in vitro degradation behavior of Mg-6Zn alloy studied by electrochemical measurements [J]. Advanced Engineering Materials B. 2010. 12: 170-174.
- [18] LIU Xian-bin, SHAN Da-yong, SONG Ying-wei, HAN En-hou. Effects of heat treatment on corrosion behaviors of Mg-3Zn magnesium alloy [J]. Transactions of Nonferrous Metals Society of China, 2010, 20: 1345-1350.

- [19] AUNG N, ZHOU W. Effect of heat treatment on corrosion and electrochemical behaviour of AZ91D magnesium alloy [J]. Journal of Applied Electrochemistry, 2002, 32: 1397–1401.
- [20] MURRAY J, MASSALSKI T. Binary alloy phase diagrams [M]. Metals Park, OH: American Society for Metals, 1986.
- [21] FAN Xin, CHEN Jian, ZOU Jian-peng, WAN Qian, ZHOU Zhong-cheng, RUAN Jian-ming. Bone-like apatite formation on HA/316L stainless steel composite surface in simulated body fluid [J]. Transactions of Nonferrous Metals Society of China, 2009, 19: 347–352
- [22] ZENG Rong-chang, HU Yan, GUAN Shao-kang, CUI Hong-zhi, HAN En-hou. Corrosion of magnesium alloy AZ31: The influence of bicarbonate, sulphate, hydrogen phosphate and dihydrogen phosphate ions in saline solution [J]. Corrosion Science, 2014, 86: 171–182.
- [23] WANG Y, LIU G, FAN Z. Microstructural evolution of rheo-diecast AZ91D magnesium alloy during heat treatment [J]. Acta Materialia, 2006. 54: 689–699
- [24] SHI Zhi-ming, LIU Ming, ATRENS A. Measurement of the corrosion rate of magnesium alloys using Tafel extrapolation [J]. Corrosion Science, 2010, 52: 579–588.
- [25] XIN Yun-chang, HUO Kai-fu, TAO Hu, TANG Guo-yi, CHU P K. Influence of aggressive ions on the degradation behavior of biomedical magnesium alloy in physiological environment [J]. Acta Biomaterialia, 2008, 4: 2008–2015.
- [26] YAMAMOTO A, HIROMOTO S. Effect of inorganic salts, amino acids and proteins on the degradation of pure magnesium in vitro [J]. Materials Science and Engineering C, 2009, 29: 1559–1568.
- [27] YANG Lei, ZHANG Er-lin. Biocorrosion behavior of magnesium alloy in different simulated fluids for biomedical application [J]. Materials Science and Engineering C, 2009, 29: 1691–1696.
- [28] ATRENS A, LIU M, ABIDIN N I Z. Corrosion mechanism applicable to biodegradable magnesium implants [J]. Materials Science and Engineering B, 2011, 176: 1609–1636.

# 固溶处理对可生物降解 Mg-6Zn 合金腐蚀性能的影响

Seyed Morteza Ghaffari SHAHRI<sup>1</sup>, Mohd Hasbullah IDRIS<sup>1</sup>, Hassan JAFARI<sup>2</sup>, Babak GHOLAMPOUR<sup>1</sup>, Mahtab ASSADIAN<sup>1</sup>

- 1. Department of Materials, Manufacturing and Industrial Engineering, Faculty of Mechanical Engineering, Universiti Teknologi Malaysia, Johor Bahru 81310, Malaysia;
  - Department of Materials Engineering, Faculty of Mechanical Engineering, Shahid Rajaee Teacher Training University, Tehran, 16785-136, Iran

摘 要: 对可生物降解二元 Mg–6Zn 合金进行固溶处理,来评价获得的显微组织变化对合金降解速率的影响及其相关机理。在 350 °C 条件下固溶处理 6~48 h。采用光学显微镜、扫描电镜、能量色散 X 射线光谱仪和 X 射线衍射仪分析铸态和固溶处理后试样。在 37 °C 的模拟体液中进行浸泡和电化学测试,评价其抗腐蚀性。为保证腐蚀测试的结果,对 pH 值进行测试。结果发现,大于 24 h 的固溶处理,金属间化合物相溶解于基体中,并产生了近单晶相组织。金属间化合物相的减少导致阴极区/阳极区比减小且腐蚀率降低。电化学和失重测试结果表明,延长固溶处理时间可提高合金的抗腐蚀性。经 350 °C 固溶处理 24 h 后,铸态合金的抗腐蚀性提高了 60%以上。另外,逐渐减少的金属间化合物相和伴随的低 pH 值上升,降低了腐蚀速率。对于 Mg–Zn 合金作为生物可降解移植材料的应用,固溶处理是一种可以提高腐蚀性的工艺。

关键词: 镁合金; 固溶处理; 生物降解; 浸泡; 极化; 矫形外科植入